Journal of Materials Chemistry A

Accepted Manuscript

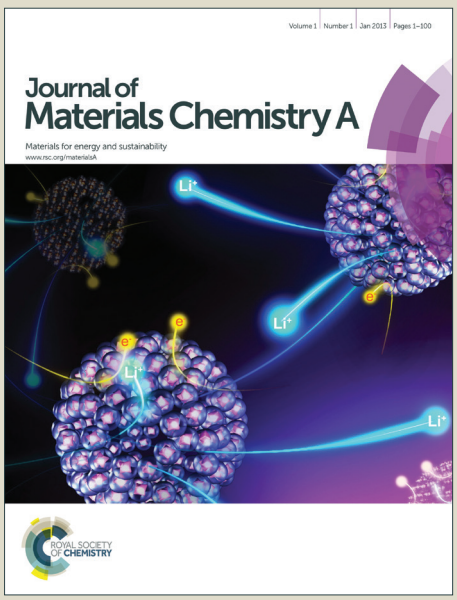

ROYAL SOCIETY OF CHEMISTRY

www.rsc.org/materialsA

Journal Name

RSCPublishing

ARTICLE

Highly Ordered Mesoporous $NiCo_2O_4$ with Superior Pseudocapacitance Performance for Supercapacitors

Cite this: DOI: 10.1039/x0xx00000x

Lei An[a], Qilong Ren[a], Wenyao Li[a,b], Kaibing Xu[a], Yunjiu Cao[a,c], Tao Ji[a,c], Rujia Zou[a,d], Zhigang Chen[a], and Junqing Hu*[a]

Received 00th January 2012,
Accepted 00th January 2012

DOI: 10.1039/x0xx00000x

www.rsc.org/

Conventional $NiCo_2O_4$ without mesopores prepared by direct thermal decomposition of appropriate mixture solution consisting of $Co(NO_3)_2\ 6H_2O$ and $Ni(NO_3)_2\ 6H_2O$ does not provide superior pseudocapacitance performance due to the inadequate redox reaction during charge and discharge process when used as an electrode material for pseudocapacitors. In this work, we demonstrate the synthesis of highly ordered mesoporous $NiCo_2O_4$ by nanocasting method and examine its electrochemical performance by means of cyclic voltammetry and galvanostatic charge-discharge method. The highly ordered mesoporous $NiCo_2O_4$ prepared using mesoporous silica KIT-6 as a template presents exceptionally high specific capacitance (1699 F g^{-1} at a current density of 1 A g^{-1}) and an excellent cycling ability (~ 104.1% retention after 10000 cycles). In addition, other 3D mesoporous nanostructures (mesoporous Co_3O_4 and mesoporous NiO) synthesized by similar nanocasting method also show outstanding pseudocapacitive performance. Thus, the effective design of highly ordered mesoporous electrodes demonstrated in this work offers a promising strategy for supercapacitors with superior electrochemical properties.

Introduction

With the fast-increasing growth of portable electronics and hybrid electric vehicles, the requirement for high-power energy resources has increased dramatically in recent years. Electrochemical capacitors, also known as supercapacitors, have drawn great interest as the most promising candidates for next-generation high-capacitance energy storage devices due to their high specific power, environmental friendliness and longer lifespan [1-7]. According to the previously reported charge-storage mechanism, electrochemical capacitors mainly can be divided into two major types: electrical double-layer capacitors (EDLCs) and pseudocapacitors [8-10]. Complementary to EDLCs via reversible ion absorption at the electrode/electrolyte interfaces to store charges, pseudocapacitors using redox-active materials utilize fast and reversible Faradaic reactions that take place on electrode surfaces, thus furnishing observably higher specific capacitance than EDLCs [10-13].

For pseudocapacitors, electrode material plays a vital role on the electrochemical property. Among various electrode materials, spinel nickel cobaltite ($NiCo_2O_4$) has been widely investigated as advanced electrode materials owing to its better electronic conductivity (two orders of magnitude higher than conventional transition metal oxides), low cost, high availability, and good corrosion resistance in alkaline solutions [14-17]. Many reports are available on the preparation and electrochemical properties of the $NiCo_2O_4$ electrode material with various nanostructures, such as porous spheres (856 F g^{-1} at 1 A g^{-1}) [18], nanorods (565 F g^{-1} at 1 A g^{-1}) [19], nanowires (743 F g^{-1} at 1 A g^{-1}) [20], and flowerlike nanostructure (658 F g^{-1} at 1 A g^{-1}) [21]. Unfortunately, in these cases above the observed specific capacitances are far from satisfactory as the diffusion distance of electrolytes into pseudocapacitor electrodes is only ~ 20 nm and active materials over this distance can't make a contribution to the total capacitance adequately during charge/discharge process [22, 23].

Introducing mesopores in transition metal oxides can be an efficient strategy to improve the utilization of active material, thereby resolving problems concerned about reversible redox Faradaic reactions and alleviating the volume change during charge/discharge processes [24]. It has been found that the reported specific capacitance and lifespan are dramatically improved by mesoporous nanostructure of the active material electrodes [25-27], since the thin pore wall can lessen the electrolyte ion diffusion path. Porous microstructures of transition metal oxides have been proposed to be obtained via the nanocasting [28], hydrothermal method [29], chemical bath precipitation [30], electrochemical deposition [31], and thermal decomposition methods [32]. Among these methods, nanocasting can offer the opportunity to obtain materials which are different from each other with respect to mesoporous structure. Moreover, active materials prepared through nanocasting can increase active sites vastly and engage in the reversible faradic reaction adequately when used as electrodes for pseudocapacitors. Furthermore, to minimize the diffusion length of charge carriers is crucial adjective for elevating the performance of pseudocapacitance performance. Therefore, rational design of electrode materials with mesoporous

nanostructure by nanocasting is indispensable for the further improvement of the pseudocapacitive properties.

In this work, we report the synthesis of highly ordered mesoporous $NiCo_2O_4$ and test its electrochemical performance as an electrode material for pseudocapacitors by means of cyclic voltammetry and galvanostatic charge-discharge method and compared the results with those of conventional $NiCo_2O_4$ without mesoporous nanostructure. The results demonstrate that the $NiCo_2O_4$ with mesoporous nanostructure exhibits high specific capacitance (1699 F g^{-1} at a current density of 1 A g^{-1}) and predominant cycling lifespan (~ 104.1% retention after 10000 cycles), indicating that $NiCo_2O_4$ with mesoporous nanostructure is a promising active electrode material for advanced supercapacitors. Giving extended application, we synthesized other similar 3D mesoporous nanostructures (mesoporous Co_3O_4 and mesoporous NiO), also demonstrating outstanding pseudocapacitive properties.

Experimental Characterization

All the chemicals were of analytical grade and used without further purification.

Synthesis of Mesoporous Silica KIT-6

The mesoporous KIT-6 was prepared according to a literature procedure [33]. A typical synthesis procedure was as follows: 4.5 g of surfactant pluronic 123 ($EO_{20}PO_{70}EO_{20}$) was dissolved in a mixture solution of 163 mL of distilled water and 7.5 mL of concentrated HCl (37%). The above mixture was stirred at 35 ℃ until a homogeneous solution was obtained. Then, 4.5 g of n-Butanol was added to the homogeneous solution. After 1 h of stirring the mixture, 9.675 g of tetraethoxysilane (TEOS) was added to the solution, and stirring was continued at the same temperature for another 24 h. After that, the mixture was aged at 35 ℃ for 24 h. The final solid product was filtered, dried at 90 ℃, and finally the dried product was calcined at 550 ℃ for 6 h under a heating rate of 2 ℃ min^{-1} for the removal of P-123 block copolymer.

Preparation of Mesoporous $NiCo_2O_4$.

0.4 g of KIT-6 was dispersed in 4 mL of 1 M $Co(NO_3)_2$•$6H_2O$ and 2 mL of 1 M $Ni(NO_3)_2$•$6H_2O$ in ethanol. The mixture was stirred for 1.5 h in a crucible and left for ethanol evaporation at 70 ℃ till the mixture was dried. Subsequently, the as-formed powder was calcined at 200 ℃ for 4 h under a heating rate of 2 ℃ min^{-1}. The impregnation step was repeated one more times with 2 mL of 1 M $Co(NO_3)_2$•$6H_2O$ and 1 mL of 1 M $Ni(NO_3)_2$•$6H_2O$ in ethanol with the same calcination procedure. Then, a further calcination at 450 ℃ for 6 h under a heating rate of 1 ℃ min^{-1} was conducted. The silica host was removed with 25 mL of 2 M NaOH solution at 60 ℃ under stirring for 24 h. The $NiCo_2O_4$ replica was filtered and washed with deionized water and absolute ethanol for several times, then dried at 60 ℃ overnight. The conventional $NiCo_2O_4$ was prepared by directly calcining the mixture solution (6 mL of 1 M $Co(NO_3)_2$•$6H_2O$ and 2 mL of 1 M $Ni(NO_3)_2$•$6H_2O$ in ethanol) without adding KIT-6 at 450 ℃ for 6 h.

Characterization

X-ray diffraction (XRD) patterns of all the samples were carried out with D/max-2550 PC X-ray diffractometer (XRD; Rigaku, Cu-Kα radiation). The surface area, pore size, and pore-size distribution of the as-prepared products were determined by Brunauer-Emmett-Teller (BET) nitrogen adsorption-desorption and Barrett-Joyner-Halenda (BJH) methods (Micromeritics, ASAP2020). The morphology of the materials was examined by a scanning electron microscope (SEM; S-4800) and a transmission electron microscope (TEM; JEM-2010F) equipped with an energy dispersive X-ray spectrometer (EDX). The mass of electrode materials was weighed on a XS analytical balance (Mettler Toledo; δ = 0.01 mg).

Electrochemical measurement

Electrochemical measurements were carried out using electrochemical workstation (Autolab PGSTAT302N potentiostat, Switzerland) with a three-electrode mode in a 6 M KOH solution. The working electrode is consisted of active material, carbon black and polymer binder (polyvinylidene fluoride; PVDF) with a weight ratio of 80: 15: 5 and stirred for 24 h. For pseudocapacitance test, the slurry was pasted to Ni foam and then dried at 120 ℃ for 6 h under vacuum to remove the solvent. After that, the as-formed electrodes were pressed at 10 MPa. The loading mass was about 1.49 and 1.65 mg for mesoporous $NiCo_2O_4$ and conventional $NiCo_2O_4$, respectively. A saturated calomel electrode (SCE) was used as the reference electrode and a platinum (Pt) sheet electrode was used as the counter electrode. All potentials were referred to the reference electrode. The specific capacitance and current density were calculated based on the mass of these electroactive materials.

Results and discussion

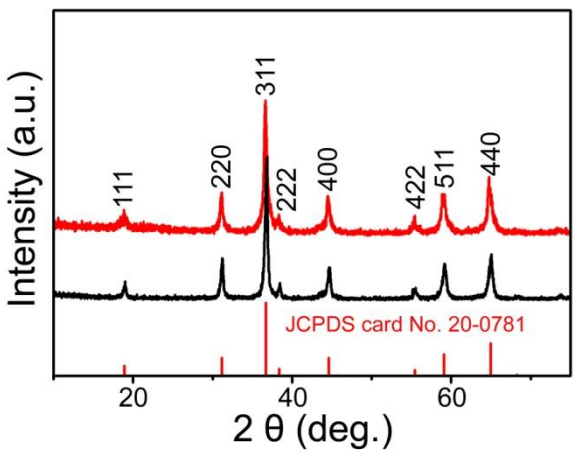

Fig. 1 XRD patterns of the mesoporous $NiCo_2O_4$ and conventional $NiCo_2O_4$

To determine the phase structures, the X-ray diffraction (XRD) measurements of the products were performed. In Figure 1, all diffraction peaks of the mesoporous $NiCo_2O_4$ material can be unambiguously assigned to $NiCo_2O_4$ phase (JCPDS card no.: 20-0781) (red line). No peaks from other phases are detected, indicating that the as-prepared products are of high purity. XRD patterns of the corresponding conventional $NiCo_2O_4$ were also detected and there's no distinct difference in peak position of the two materials.

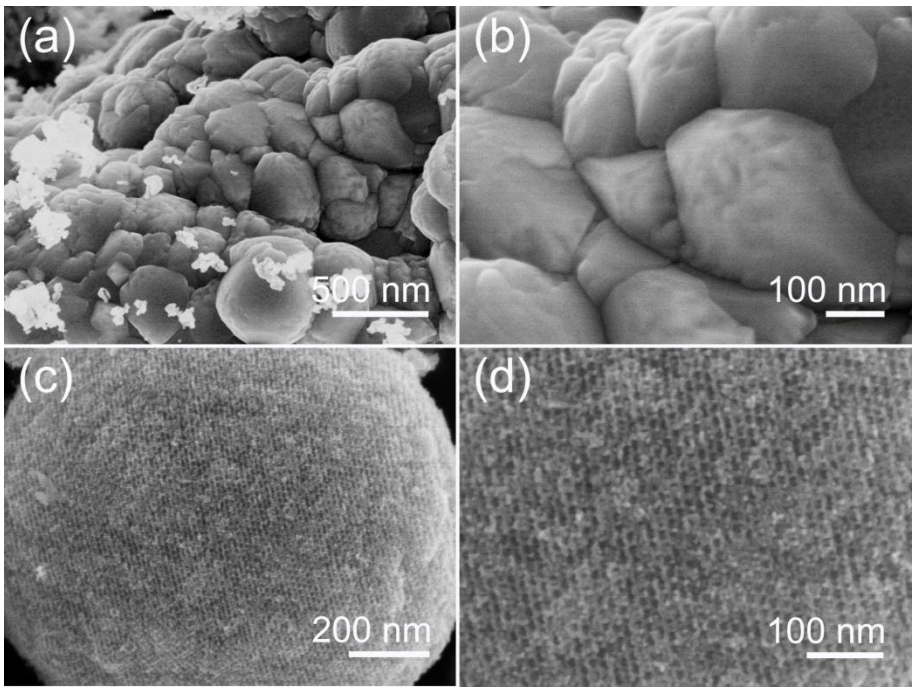

Fig. 2 Different magnification SEM images of (a, b) the conventional $NiCo_2O_4$ and (c, d) the mesoporous $NiCo_2O_4$, respectively.

The microstructure and morphology of the mesoporous $NiCo_2O_4$ were studied by utilizing a scanning electron microscopy (SEM). The SEM images of the mesoporous $NiCo_2O_4$ were compared with the conventional $NiCo_2O_4$. Fig 2a, b show the conventional $NiCo_2O_4$, in which it consists of larger particles with very smooth surface, while Fig. 2c, d demonstrate different magnification SEM images of the mesoporous $NiCo_2O_4$. It was found that a highly ordered mesostructure can be clearly observed and that the surface of the particle is quite rough, indicating that the mesostructure regularity is well preserved after the nanocasting replication and almost all of the precursor solutions were filled into the mesopores of the KIT-6 and in-situ transformed to $NiCo_2O_4$ during the preparation. The special sub-framework structure can exhibit a unique feature with reasonable intervals among adjoining nanostructures. Thus, we can anticipate that the as-synthesized microstructures can access to the electrolyte highly and participate in the pseudocapacitance reaction adequately due to the presence of convenient diffusion paths when used as an electrode for supercapacitors, while the conventional $NiCo_2O_4$ without mesopores may prevent the microstructures of the conventional material from fully contacting the electrolyte when used as an electrode.

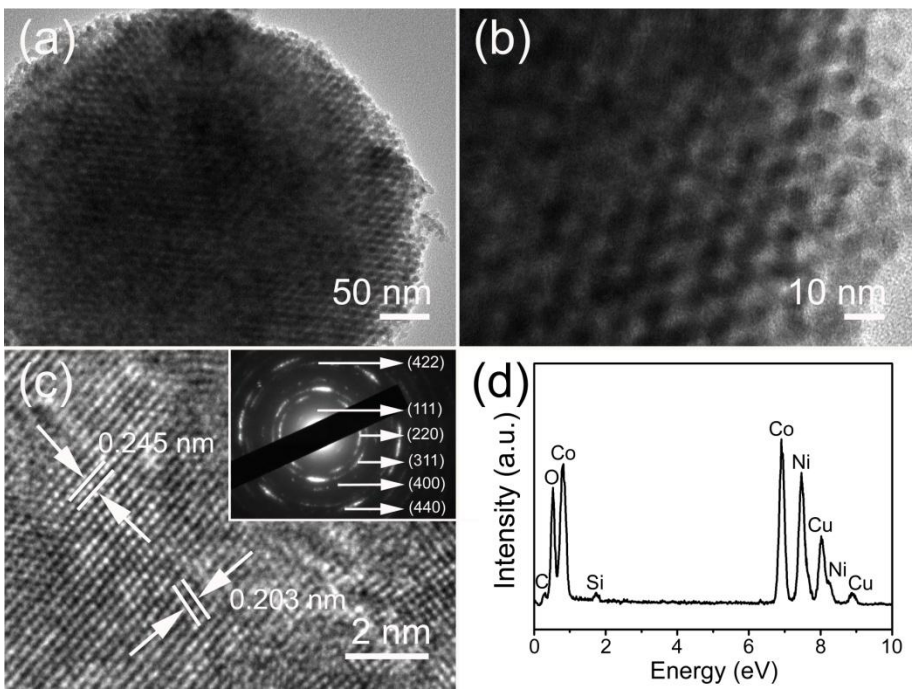

Fig. 3 Typical TEM images (a-c) and EDX pattern (d) taken from crystalline mesoporous $NiCo_2O_4$. The inset in (c) is the corresponding SAED pattern.

The replication of the KIT-6 silica by $NiCo_2O_4$ can also be observed in the transmission electron microscopy (TEM) images directly. The three-dimensional open, well-ordered and accessible mesopores of the as-formed $NiCo_2O_4$ are clearly visible in Figure 3a, b. No large nonporous impurity particles were observed and the pure high 3D ordering presents in the particles over a long distance, indicating that almost all the cobalt nitrate solutions were successfully filled inside the mesopores and then transformed in-situ to the $NiCo_2O_4$ material. The high-resolution TEM (HRTEM) image (Fig. 3c) suggests a highly polycrystalline nature of the Co_3O_4 walls and reveals lattice fringes with interplane spacings of 0.245 and 0.203 nm, corresponding to the distance of the (211) and (400) planes of the $NiCo_2O_4$ crystal, respectively. The corresponding selected-area electron diffraction (SAED) pattern (inset of Fig. 2c) shows well-defined diffraction rings, also suggesting their polycrystalline characteristics. In order to better understand the chemical composition of the as-prepared product, the energy dispersive X-ray (EDX) spectrometer characterization of the mesoporous $NiCo_2O_4$ were also conducted. In Figure 3d, it was found that the microstructure consists of Co, Ni, O, Cu, C and Si elements, in which Cu peaks derived from Cu grid and C element resulted from C membranes on Cu grid. Besides, Si peak originated from the residual silica and the peak intensity of Si is far less than that of the other elements which can be negligible in the chemical composition of the as-prepared materials, further indicating the formation of $NiCo_2O_4$ crystal.

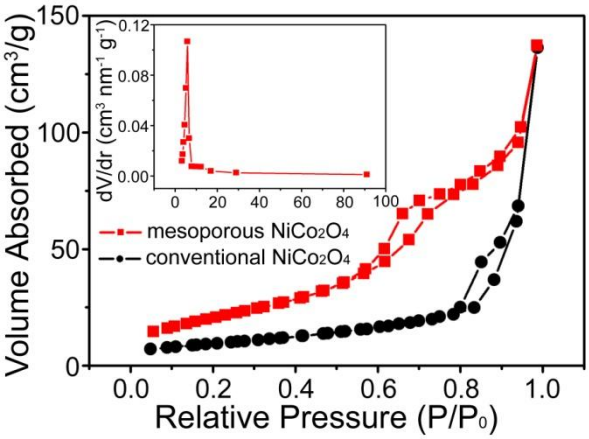

Fig. 4 The nitrogen adsorption-desorption isotherm of the mesoporous $NiCo_2O_4$ and conventional $NiCo_2O_4$, respectively. The inset shows the corresponding BJH pore size distribution plots of the mesoporous $NiCo_2O_4$.

In terms of mesoporosity, the replication of the KIT-6 silica by $NiCo_2O_4$ was investigated by the N_2 adsorption-desorption isotherm, as shown in Fig. 4. The isotherm is of type IV of the IUPAC classification with typical hysteresis loop. $NiCo_2O_4$ has a BET surface area of 87 m^2 g^{-1}, which is much larger than that of the conventional $NiCo_2O_4$ with a surface area of 33.86 m^2 g^{-1}. The hysteresis loop in the isotherm indicates the presence of mesopores in the as-prepared samples, as further shown in the Barrett-Joyner-Halenda (BJH) pore size distribution curves (inset of Fig. 4). Mesoporous $NiCo_2O_4$ exhibits unique porous structure and both of the average pore size is ~ 5.8 nm. It is worth mentioning that the three-dimensional open, well-ordered and accessible mesopores connected to each other inside the unique microstructure can act as "ion reservoir" that can reduce the diffusion distance from the penetrating electrolyte to the interior surfaces when used as electrodes.

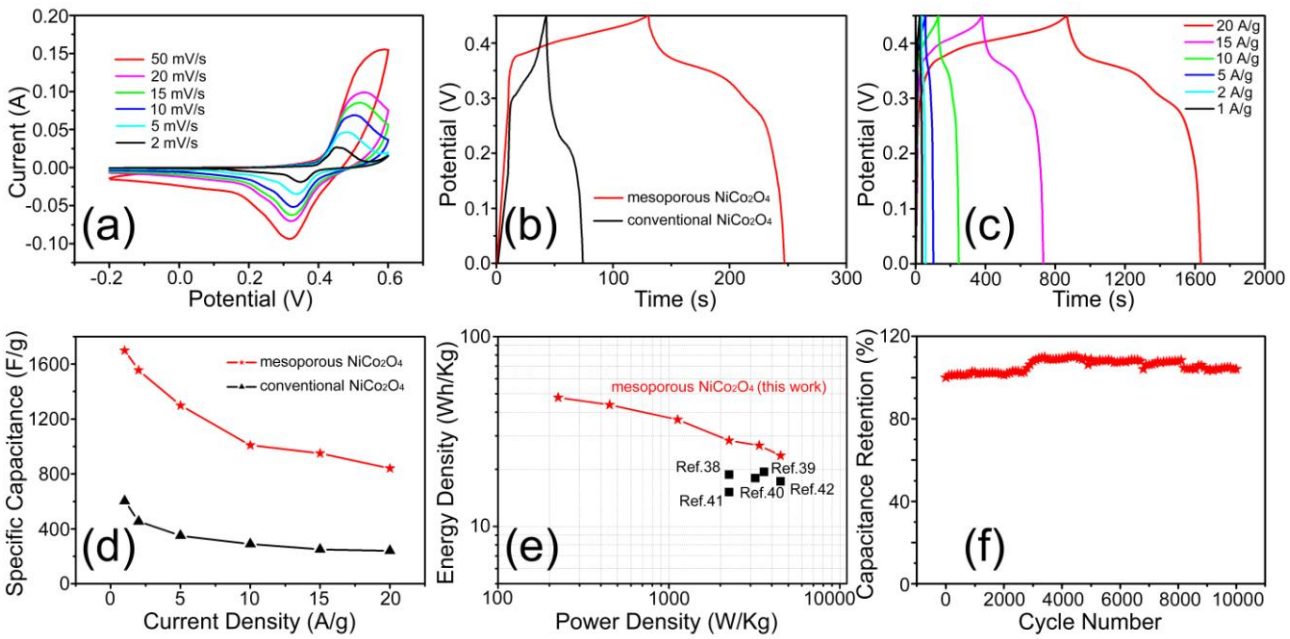

Fig. 5 (a) CV curves of the mesoporous $NiCo_2O_4$ and conventional $NiCo_2O_4$ at different scan rates. (b) Galvanostatic charge-discharge curves at a current density of 5 A g^{-1} of the mesoporous $NiCo_2O_4$ and conventional $NiCo_2O_4$, respectively. (c) Galvanostatic charge-

discharge curves at different current densities of the mesoporous $NiCo_2O_4$. (d) Specific capacitance at different current densities and (e) Ragone plot (energy density vs. power density) of the mesoporous $NiCo_2O_4$ in comparison with energy densities at maximum power densities of other work. (f) Variation of specific capacitance with cycle number at a scan rate of 50 mV s^{-1} of the mesoporous $NiCo_2O_4$.

As described above, $NiCo_2O_4$ material with unique mesoporous microstructure can be synthesized by the facile hard template method. It will be attractive to study the electrochemical performance of the as-synthesized active material. The $NiCo_2O_4$ microstructure is studied as electrode in a three-electrode configuration with 6 M KOH as the electrolyte for supercapacitor. Fig. 5a shows the cyclic voltammetry (CV) curves of the mesoporous $NiCo_2O_4$ at different scan rates in the voltage window between 0 and 0.6 V. All curves reveal that the capacitive characteristics are different from those of electrochemical double-layer capacitors. A pair of redox couples is deserved in the CV curve, which is mainly associated with the Faradaic redox reactions related to M-O/M-O-OH, where M refers to Ni or Co [34, 35]. Interestingly, with the scan rate increasing from 2 to 50 mV/s the redox current increased. Also, the oxidation and reduction peaks shifted toward higher and lower potentials, respectively, with a large potential separation. Similar phenomenon was also observed in the conventional $NiCo_2O_4$ (Fig. S1a). The mesoporous $NiCo_2O_4$ and conventional $NiCo_2O_4$ were also characterized using galvano-static charge/discharge measurements. Fig. 5b shows the charge-discharge curves of the mesoporous $NiCo_2O_4$ and conventional $NiCo_2O_4$ at a current density of 5 A g^{-1}. It can be seen that the charge curve of the mesoporous $NiCo_2O_4$ is not strictly but approximately symmetric to its corresponding discharge counterpart, indicating the good reversibility of the as-formed material. It is worthy to note that the specific capacitance of the mesoporous $NiCo_2O_4$ can reach 1299 F g^{-1}, which is over three times higher than that of the conventional $NiCo_2O_4$ (350 F g^{-1}). Further galvanostatic CD investigations of the mesoporous $NiCo_2O_4$ and conventional $NiCo_2O_4$ between 0 and 0.45 V at different current densities are shown in Fig. 5c and Fig. S1b. The specific capacitances of the mesoporous $NiCo_2O_4$ are also higher than those of the conventional $NiCo_2O_4$ at other current densities. The calculated specific capacitance as a function of the discharge current density is plotted in Fig. 5d. It is worth mentioning that the specific capacitance of the mesoporous $NiCo_2O_4$ at 1, 2, 5, 10, 15 and 20 A/g is 1699, 1556, 1299, 1009, 950 and 840 F g^{-1}, respectively, which is higher than that of the conventional $NiCo_2O_4$ (602 F g^{-1} and 240 F g^{-1} at current densities of 1 A g^{-1} and 20 A g^{-1}, respectively). The performance of the mesoporous $NiCo_2O_4$ is remarkable compared with other reported $NiCo_2O_4$ electrodes in previous literature, as summarized in Table S1. The specific capacitance of the mesoporous $NiCo_2O_4$ is much higher than these reported $NiCo_2O_4$, which is contributed to the unique microstructure possessing high surface area. Fig. 5e in the main text (i.e., Fig. 1e here) shows the Ragone plots of the $NiCo_2O_4$ electrode based on the galvano-static charge/discharge measurements at the potential window of 0-0.45 V. As a comparison, these energy densities at maximum power densities from other reported $NiCo_2O_4$ electrodes were also provided here. It is worth noting that the maximum energy density of our mesoporous $NiCo_2O_4$ electrode is 47.78 Wh kg^{-1} at a power density of 225 W kg^{-1} (Shown in Fig. S2), which is almost 3 times larger than that of the conventional $NiCo_2O_4$ (16.94 Wh kg^{-1}) and is also significantly higher than those of the reported $NiCo_2O_4$ based electrode materials.[38-42] In addition, the cycling stability is also conducted by the repeated charging-discharging measurement at a scan rate of 50 mV s^{-1}, as shown in Fig. 5f. The final specific capacitance of the mesoporous $NiCo_2O_4$ retained 104.1 % of its initial value after 10000 cycles. In other words, the loss in specific capacitance based on the maximum value is only 5.4 %, which is considered outstanding performance for $NiCo_2O_4$ microstructures.

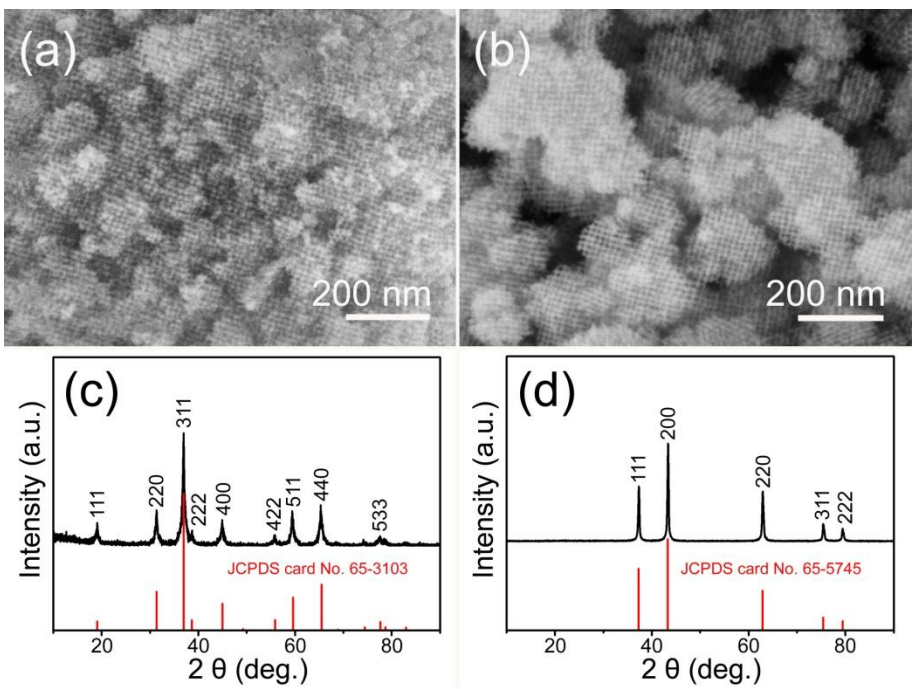

Fig. 6 (a, b) SEM images and (c, d) XRD patterns of 3D mesoporous Co_3O_4 and 3D mesoporous NiO nanomaterials, respectively.

Other similar 3D mesoporous nanostructures, like mesoporous Co_3O_4 and NiO were also synthesized by controlling the precursors or reaction temperature. In Fig. 6a, b, a highly ordered mesostructure can be clearly observed for the two product particles, indicating that the mesostructures regularity are well preserved after the nanocasting replication. The phases of the as-prepared samples were

examined by the XRD, as shown in Fig. 6c, d. All of the diffraction peaks of both samples can be unambiguously assigned to their corresponding standard phase (JCPDS card no.: 65-3101 and JCPDS card no.: 65-5745).

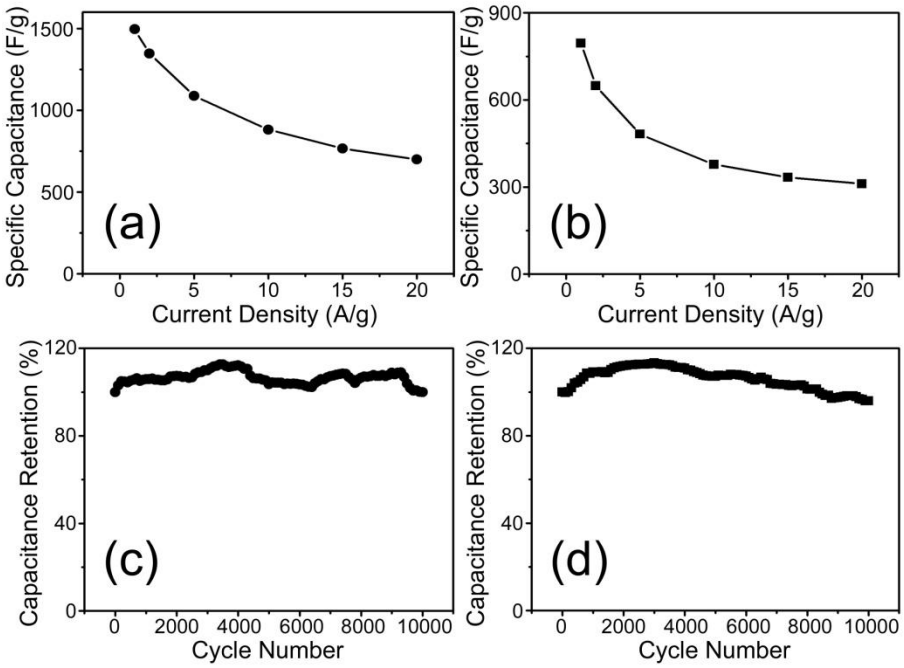

Fig. 7 Specific capacitance at different current densities (a, b) and variation of specific capacitance with cycle number at a scan rate of 50 mV s^{-1} (c, d) of the mesoporous Co_3O_4 and mesoporous NiO, respectively.

It is also anticipating to investigate the electrochemical performances of the as-formed mesoporous Co_3O_4 and NiO nanostructures. Fig. S3a, b shows the typical CV curves of the mesoporous Co_3O_4 and NiO nanostructure electrodes with their corresponding various sweep rates. Similarly, the shape of the CV curves of these two nanostructures clearly also reveal their pseudocapacitive characteristics. Fig. S3c, d show the constant current charge/discharge profiles at different current densities of these two nanostructures, respectively. The calculated specific capacitance as a function of the discharge current density is plotted in Fig. 7a, b. Notably, the specific capacitance is as high as 1496, 1348, 988, 782, 667 and 600 F g^{-1} (for mesoporous Co_3O_4) and 796, 649, 482, 378, 333 and 311 F g^{-1} (for mesoporous NiO) at the discharge current densities of 1, 2, 5, 10, 15 and 20 A g^{-1}, respectively. In addition, their cycling stabilities are also evaluated by the repeated charging-discharging measurement at a scan rate of 50 mV s^{-1}, as shown in Fig. 7c, d. The final specific capacitance can be retained to be 100.02 % (for mesoporous Co_3O_4) and 95.9 % (for mesoporous NiO) of their corresponding initial value after 10000 cycles, respectively.

The above electrochemical measurements demonstrate that the unique mesoporous microstructures based on $NiCo_2O_4$, Co_3O_4, and NiO can deliver outstanding specific capacitance with remarkable cycling stability. The fascinating electrochemical properties could be related to the following morphology and structure features. Firstly, the mesoporous nano-sized walls can greatly increase electroactive sites and make active materials fully get access to the KOH electrolyte. Secondly, the reasonable room among interconnected crystalline walls allows for easy diffusion of the electrolyte into the inner region of the electrodes. Thirdly, the thin walls can result in short paths for electron transport and species diffusion. In addition, the strong 3D mesoporous architecture can sustain huge structural alteration during the lengthy charge/discharge processes. Thus, these as-synthesized unique microstructures can participate in the reversible faradic reaction adequately and deliver exceptional pseudocapacitive properties. When compared with the mesoporous Co_3O_4 or NiO electrode, it can be clearly seen that the mesoporous $NiCo_2O_4$ sample exhibits better pseudocapacitive performance with both higher capacitance and better cycling stability. We can understand the difference based on the reported result that $NiCo_2O_4$ possesses a better electronic conductivity and higher electrochemical activity than Co_3O_4 and NiO [43-45], This achievement can be further confirmed by electrochemical impedance spectroscopy (EIS). From the Nyquist plots (Fig. S4), it can be observed that the magnitude of ESR originated from the mesoporous $NiCo_2O_4$ electrode (0.33 Ω) is smaller than that of the mesoporous Co_3O_4 electrode (0.59 Ω) and mesoporous NiO electrode (0.80 Ω).

Conclusions

In summary, highly ordered mesoporous $NiCo_2O_4$ was prepared by nanocasting for high-performance pseudocapacitors. The well-ordered mesoporous $NiCo_2O_4$ as electrode materials delivered an outstanding specific capacitance of 1699 F g^{-1} at a current density of 1 A g^{-1}, which is superior to 602 F g^{-1} of the conventional $NiCo_2O_4$ at the same current density. Moreover, the highly ordered mesoporous electrode microstructure also exhibited an ultrahigh lifespan (~ 104.1% retention of the initial capacitance after 10000 cycles) for pseudocapacitors, indicating that $NiCo_2O_4$ with highly ordered mesoporous nanostructure is a promising active electrode material. In addition, we tried to synthesize other similar 3D mesoporous nanostructures, mesoporous Co_3O_4 and mesoporous NiO, also demonstrating outstanding pseudocapacitive properties. The effective design of highly ordered mesoporous electrodes can furnish a fantastic approach for pseudocapacitors with uncontemplated electrochemical performance.

Acknowledgements

This work was financially supported by the National Natural Science Foundation of China (Grant Nos. 51472049, 51302035, and 21171035), the National 863 Program of China (Grant No. 2013AA031903), the Key Grant Project of Chinese Ministry of Education (Grant No. 313015), Ph.D. Programs Foundation of Ministry of Education of China (Grant Nos. 20110075110008 and 20130075120001), the Science and Technology Commission of Shanghai Municipality (Grant No. 13ZR1451200), the Hong Kong Scholars Program, Fundamental Research Funds for the Central Universities, the Shanghai Leading Academic Discipline Project (Grant No. B603), and the Program of Introducing Talents of Discipline to Universities (Grant No. 111-2-04). the graduate students scientific research innovation projects of Shanghai university of engineering science (14KY0512), and the 2012 special fund of development of science and technology of Shanghai university of engineering science (2013gp19).

Notes and references

a State Key Laboratory for Modification of Chemical Fibers and Polymer Materials, College of Materials Science and Engineering, Donghua University, Shanghai 201620, China.
b School of Material Engineering, Shanghai University of Engineering Science, Shanghai 201620, China.
c School of Fundamental Studies, Shanghai University of Engineering Science, Shanghai 201620, China.
d Center of Super-Diamond and Advanced Films (COSDAF), Department of Physics and Materials Science, City University of Hong Kong, Hong Kong.

E-mail: hu.junqing@dhu.edu.cn.

Electronic Supplementary Information (ESI) available. See DOI: 10.1039/b000000x/

1 Y. W. Zhu, S. Murali, M. D. Stoller, K. J. Ganesh, W. W. Cai, P. J. Ferreira, A. Pirkle, R. M. Wallace, K. A. Cychosz, M. Thommes, D. Su, E. A. Stach and R.S. Ruoff, *Science*, 2011**,** **332**, 1537.
2 P. Simon and Y. Gogotsi, *Nat. Mater.*, 2008, **7**, 845.
3 M. Ghidiu, M. R. L, M. Q. Zhao, Y. Gogotsi and M. W. Barsoum, *Nature*, 2014, doi:10.1038/nature13970.
4 G. G. Eshetu, M. Armand, B. Scrosati and S. Passerini, *Angew. Chem. Int. Ed.* 2014, **53**, 13342.
5 J. R. Miller and P. Simon, *Science*, 2008, **321**, 651.
6 F. Béguin, V. Presser, A. Balducci and E. Frackowiak, *Adv Mater.*, 2014, **26**, 2219.
7 J. W. Xiao, L. Wan, S. H. Yang, F. Xiao and S. Wang, *Nano Lett.*, 2014, **14**, 831.
8 R. Yi, S. R. Chen, J. X. Song, M. L. Gordin, A. Manivannan and D. H. Wang, *Adv. Funct. Mater.* 2014, **24**, 7433.
9 Z. Wu, X. L. Huang, Z. L. Wang, J. J. Xu, H. G. Wang and X. B. Zhang, *Sci Rep.*, 2014, doi:10.1038/srep03669.
10 J. P. Liu and J. Jiang; C. W. *Adv Mater.*, 2011, **23**, 2076.
11 Z. L. Ma, X. B Huang, S. Dou, J. H. Wu and S. Y. Wang, *J. Phys. Chem. C*, 2014, **118**, 17231.
12 X. H Lu, T. Zhai, X. G. Zhang, Y. Q. Shen, L. Y. Yuan, B. Hu, L. Gong, J. Chen, Y. H. Gao, J. Zhou, Y. X. Tong and Z. L. Wang, *Adv. Mater.*, 2012, **24**, 938.
13 J. W. Lee, A. S. Hall, J. D. Kim and T. E. Mallouk, *Chem. Mater.*, 2012, **24**, 1158.
14 C. Z. Yuan, J. Y. Li, L. R. Hou, X. G. Zhang, L. F. Shen and X. W. Lou, *Adv. Funct. Mater.*, 2012, **22**, 4592.
15 J. Du, G. Zhou, H. M. Zhang, C. Cheng, J. M. Ma, W. F. Wei, L. B. Chen and T. H. Wang, *ACS Appl. Mater. Interfaces*, 2013, **5**, 7405.
16 X. Y. Liu, Y. Q. Zhang, X. H. Xia, S. J. Shi, Y. Lu, X. L. Wang, C. D. Gu, J. P. Tu, *J. Power Sources*, 2013, **239**, 157.
17 Q. F. Wang, X. F. Wang, J. Xua, X. Ouyang, X. J. Hou, D. Chen, R. M. Wang and G. Z. Shen, *Nano Energy*, 2014, **8**, 44.
18 Y. R. Zhu, Z. B. Wu, M. J. Jing, H. S. Hou, Y. C. Yang, Y. Zhang, X. M. Yang, W. X. Song, X. N. Jia amd X. B. Ji, *J. Mater. Chem. A*, 2015, **3**, 866.
19 Y. R. Zhu, X. L. Pu, W. X. Song, Z. B. Wu, Z. Zhou, X. He, F. Lu, M. J. Jing, B. Tang and X. B. Ji, *J Alloys Compd.*, 2014, **617**, 988.
20 H. Jiang, J. Ma and C. Z. Li, *Chem. Commun.*, 2012, **48**, 4465.
21 H. C. Chen, J. J. Jiang, L. Zhang, T. Qi, D. D. Xia and H. Z. Wan, *J. Power Sources*, 2014, **248**, 28.
22 C. C. Hu, K. H. Chang, M. C. Lin and Y. T. Wu, *Nano Lett.*, 2006, **6**, 2690.
23 F. Z. Deng, L. Yu, G. Cheng, T. Lin, M. Sun, F. Ye and Y. F. Li, *J. Power Sources*, 2014, **251**, 202.
24 G. P. Wang, L. Zhang and J. J. Zhang, *Chem. Soc. Rev.*, 2012, **41**, 797.
25 C. H. An, Y. J. Wang, Y. N. Huang, Y. N. Xu, L. F. Jiao and H. T. Yuan, *Nano Energy*, 2014, **10**, 125.
26 Y. Huang, J. J. Liang and Y. S. Chen, *Small*, 2012, **8**, 1805.
27 J. L. Kang, A. Hirata, H. J. Qiu;, L. Y. Chen, X. B. Ge, T. Fujita and M. W. Chen, *Adv. Mater.*, 2013, **26**, 269.
28 E. Pellicer, E. Menéndez, J. Fornell, J. Nogués, A. Vantomme, K. Temst and J. Sort, *J. Phys. Chem. C*, 2013, **117**, 17084.
29 L. An, K. B. Xu, W. Y. Li, Q. Liu, Bo. Li, R. J. Zou, Z. G. Chen and J. Q. Hu, *J. Mater. Chem. A*, 2014, **2**, 12799.
30 H. B. Wu, H. Pang and X. W. Lou, *Energy Environ. Sci.*, 2013, **6**, 3619.
31 Y. M. Wang, X. Zhang, C. Y. Guo, Y. Q. Zhao, C. L. Xu and H. L. Li, *J. Mater. Chem. A*, 2013, **1**, 13290.
32 Y. F. Lee, K. H. Chang, C. C. Hu and Y. H. Chu, *J. Power Sources*, 2012, **206**, 469.
33 F. Kleitz, S. H. Choi and R. Ryoo, *Chem. Commun.*, 2003, 2136.
34 J. Pu. J. Wang. X. Q. Jin. F. L. Cui. E. H. Sheng and Z. H. Wang, *Electrochim. Acta*, 2013, **106**, 226.
35 Y. Chen. B. Qu. L. Hu. Z. Xu. Q. Li and T. Wang, *Nanoscale*, 2013, **5**, 9812.
36 Z. B. Wu, X. L. Pu, Y. R. Zhu, M. J. Jing, Q. Y. Chen, X. N. Jia, X. B. Ji, J Alloy Compd., 2015, **632**, 208.
37 Y. Lei, J. Li, Y. Y. Wang, L. Gu, Y. F. Chang, H. Y. Yuan, D. Xiao, ACS Appl. Mater. Interfaces, 2014, **6**, 1773.
38 J. Xu, L. Li, P. Gao, L. Yu, Y. Y. Chen, P. Yang, S. L. Gai and P. P. Yang, *Electrochim. Acta*, 2015, **166**, 206.
39 F. Z. Deng, L. Yu, M. Sun, T. Lin, G. Cheng, B. Lan and F. Ye, *Electrochim. Acta*, 2014, **133**, 382.
40 D. Carriazo, J. L. Patino, Maria C. Gutierrez, M. Luisa Ferrer and F. D. Monte, *RSC Adv.*, 2013, **3**, 13690.
41 C. Z. Yuan, J. Y. Li, L. R. Hou, J. D. Lin, G. Pang, L. H. Zhang, L. Lian and X. G. Zhang, *RSC Adv.*, 2013, **3**, 15873.
42 H. W. Wang, Z. A. Hu, Y. Q. Chang, Y. L. Chen, H. Y. Wu, Z. Y. Zhang and Y. Y. Yang, *J. Mater. Chem.*, 2011, **21**, 10504.
43 T. Y. Wei. C. H. Chen. H. C. Chien. S. Y. Lu and C. C. Hu, *Adv. Mater.*, 2010, **22**, 347.
44 G. Q. Zhang. H. B. Wu. H. E. Honster. M. B. Chan-Park and X. W. Lou, *Energy Environ. Sci.*, 2012, **5**, 9453.
45 H. L. Wang, Q. M. Gao and L. Jiang, *Small*, 2011, **7**, 2454.